pubs.acs.org/ac

analytical chemistry

September 2, 2014 Volume 86 Number 17

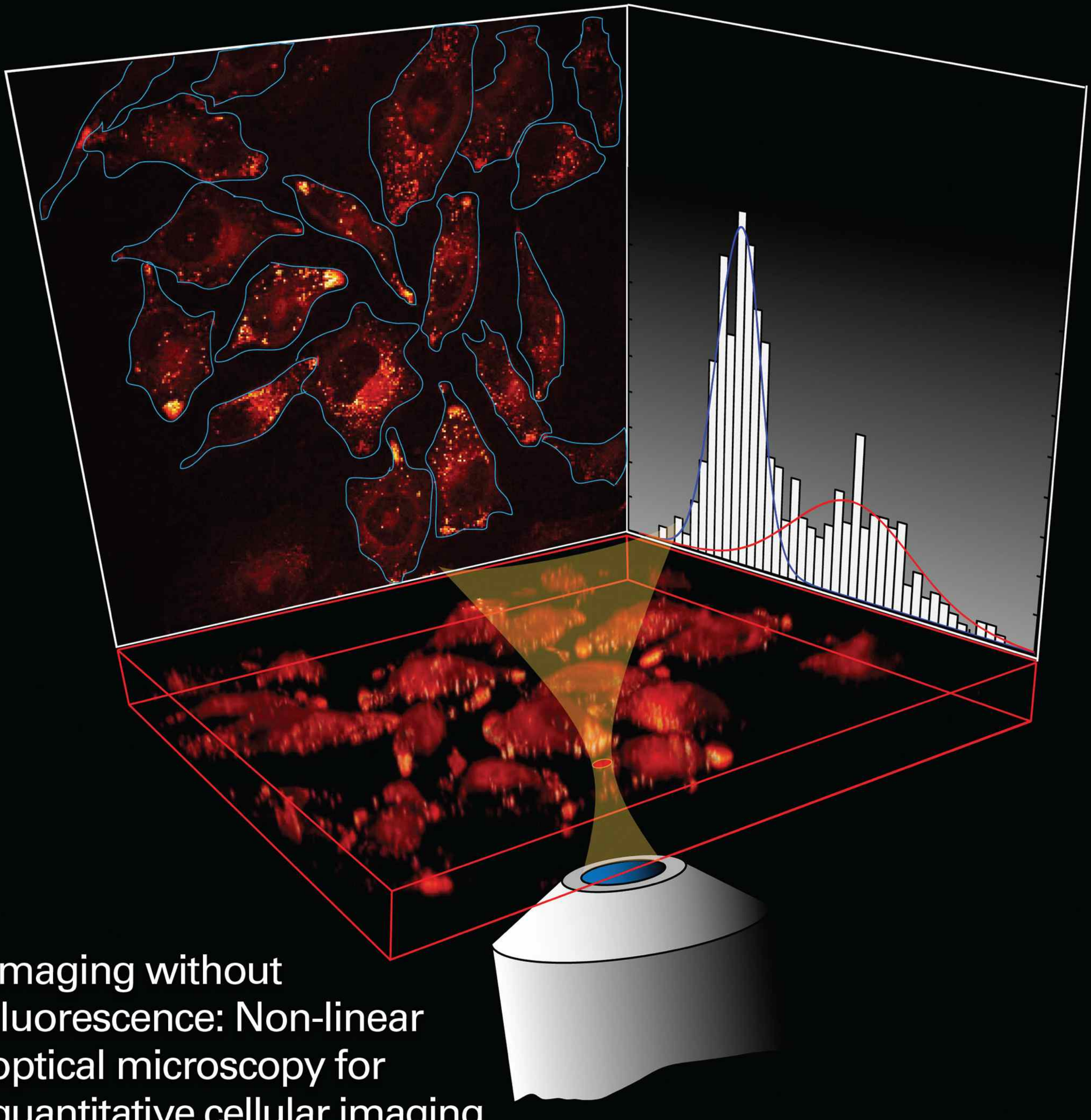

Imaging without fluorescence: Non-linear optical microscopy for quantitative cellular imaging

ACS Publications
Most Trusted. Most Cited. Most Read.

www.acs.org

analytical chemistry
Feature
pubs.acs.org/ac

Imaging without Fluorescence: Nonlinear Optical Microscopy for Quantitative Cellular Imaging

Quantitative single-cell analysis enables the characterization of cellular systems with a level of detail that cannot be achieved with ensemble measurement. In this Feature we explore quantitative cellular imaging applications with nonlinear microscopy techniques. We first offer an introductory tutorial on nonlinear optical processes and then survey a range of techniques that have proven to be useful for quantitative live cell imaging without fluorescent labels.

Aaron M. Streets, Ang Li, Tao Chen, and Yanyi Huang*

College of Engineering and Biodynamic Optical Imaging Center (BIOPIC), Peking University, Beijing, China, 100871

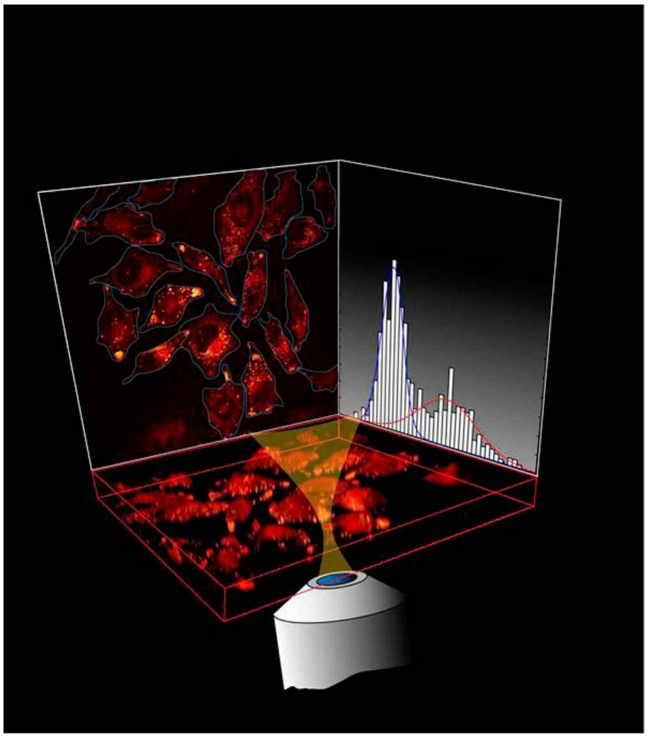

Aaron M. Streets

There has recently been a surge in applications of quantitative biological imaging, a field which has been advanced by developments in optical imaging technology as well as computational image analysis techniques. Just as the DNA sequencing revolution has enabled unprecedented understanding of biological systems at the cellular level through bioinformatic analysis, computational approaches to bioimage informatic analysis are increasingly used to extract quantitative information about the structure and dynamics of biological systems at the single-cell level using optical microscopy.

Populations of cells are inherently heterogeneous and this heterogeneity can play an important role in biological processes ranging from immune response[1] to cell fate determination.[2] In such instances, quantitative imaging and analysis at the single-cell level can provide insight into cell-to-cell variation that cannot be resolved with traditional ensemble measurement techniques. Fluorescence microscopy has been commonly used to dissect cellular heterogeneity by identifying cellular boundaries and extracting information from individual cells.[3]

In this Feature we examine a set of nonlinear optical microscopy techniques which are attractive for biological imaging applications because they can produce high-resolution, three-dimensional images of biological samples at the cellular level without the use of fluorescent labeling. When studying intercellular processes it can be advantageous to avoid labeling because large fluorescent molecules or nanomaterials may bias measurement by altering the physical or physiological properties of the molecule or system under examination. Microscopy techniques which provide chemical contrast at the cellular level without using fluorescent labels provide means to noninvasively observe the internal structure and dynamics of live cells.

Nonlinear optical microscopy exploits light−matter interactions that are intrinsic to, and often specific to, the unique optical properties of chemical compounds and structures. These techniques have demonstrated powerful applications in tissue imaging and *in vivo* diagnostics[4] in which many cells and cell types must be interrogated in unison. In these applications, low power objectives are used to image a wide field of view containing ensembles of cells for tissue characterization. Here we focus on applications which use higher magnification to distinguish single cells, probe internal cellular structure, and extract statistics from populations of cells with single cell resolution. This tutorial can be thought of as an introduction to quantitative cellular imaging beyond fluorescent labeling for analytical chemists and biologists.

■ NONLINEAR OPTICAL MICROSCOPY

Generally, imaging contrast comes from differences in the optical properties of structures within a specimen and the surrounding medium. In bright-field transmission microscopy, incident light is scattered and absorbed by a semitransparent specimen resulting in changes in intensity of the transmitted light. This light−matter interaction is fundamentally governed by the electric susceptibility of the material and at typical illumination intensities like that of a halogen lamp or most continuous wave (CW) lasers, the electromagnetic response is linear with respect to the magnitude of the incident field. With

Published: July 31, 2014

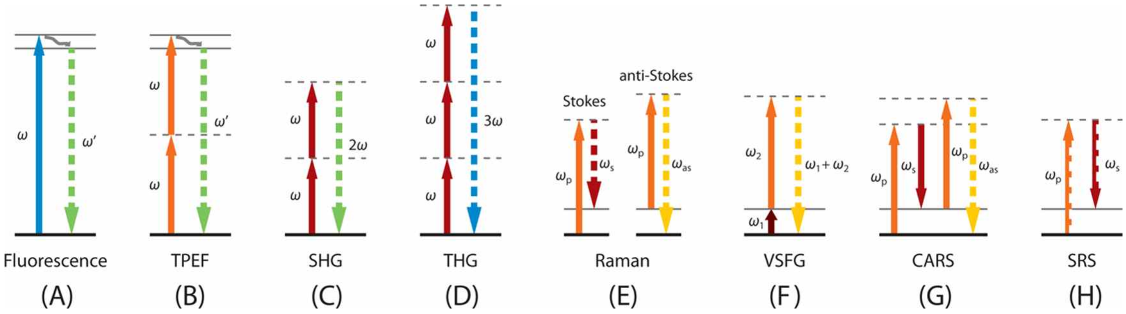

Figure 1. Energy diagrams for fluorescence and nonlinear optical processes: (A) fluorescence, (B) two-photon excitation fluorescence, (C) second harmonic generation, (D) third harmonic generation, (E) spontaneous Raman scattering, (F) vibrational sum frequency generation, (G) coherent anti-Stokes Raman scattering, and (H) stimulated Raman scattering. The thick black horizontal lines represent the ground state. Thin gray lines represent electronic or vibrational states, and dashed lines represent virtual states. Solid arrows indicate the incident beams, and dashed arrows represent the detected photons.

high incident intensities however (on the order of megawatts per square centimeter), the light−matter interaction is also governed by high-order terms in the electric susceptibility leading to a significant nonlinear response to the magnitude of the incident field. In nonlinear optical microscopy the high-order terms in the electric susceptibility, which are characteristic of the chemical compounds and structures in a sample, are exploited to provide a signal for imaging with high-intensity laser illumination.

In fact it was the invention of the laser that led to just about all of the practical discoveries and applications of nonlinear optical phenomena.[5] Many nonlinear optical processes originally found applications *within* lasers to extend light source wavelength range as well as in high-resolution spectroscopy aimed at measurement of electric susceptibilities. These techniques have since found their way into microscopy applications. Below we will briefly discuss how these fundamental nonlinear light−matter interactions have been adapted to perform biological imaging. The nonlinear optical imaging modalities we will focus on here take advantage of two major nonlinear phenomena that typically involve wavelength conversion; harmonic generation of electromagnetic radiation and radiation generated from the excitation of vibrational resonances in chemical bonds. Figure 1 displays schematic energy diagrams for the following processes and includes fluorescence and two-photon excitation fluorescence for comparison. Energy diagrams illustrate the light−matter interaction by highlighting the incident and emitted photons involved in the process.

Harmonic Generation. When electromagnetic waves interact in a nonlinear medium, the waves can mix and generate a new wave at the sum (or difference) of the original frequencies.[6] When the incident waves, or photons, are of the same frequency, the result is a new photon generated at a harmonic of the incident frequency. Second harmonic generation (SHG) occurs when two photons of the frequency ω interact inside a medium and are converted to a photon of the frequency 2ω (Figure 1C). This process is mediated by transition through a virtual energy state. Virtual states, depicted in Figure 1, are intermediate quantum states which cannot be physically occupied but enable many optical processes that would not otherwise be permitted.

Because SHG is a second order nonlinear process, it is forbidden in media with internal structure that demonstrates point centered inversion symmetry, i.e., centrosymmetric media. However, at the interface between two centrosymmetric media where such symmetry is broken or in materials with ordered noncentrosymmetric molecular organizations, SHG is allowed. Many biological structures have such molecular arrangements and therefore can produce SHG given the proper excitation field. Such structures include collagen, myofilaments, biological membranes, and quasi-crystalline tubulin assemblies such as mitotic spindles.[7−9]

Third harmonic generation (THG) is a process similar to SHG but occurs when *three* photons of the frequency ω interact inside a medium and are converted to a photon with the frequency 3ω (Figure 1D). THG does not require molecular asymmetry but instead relies on the medium's third-order electric susceptibility and finite phase matching or inhomogeneity within the excitation region. In biological samples this often occurs at the interface of two materials with otherwise homogeneous refractive indices, for example, at the surface of a cell.[10]

Vibrational Spectroscopy. Infrared spectroscopy and Raman spectroscopy are two popular techniques for acquiring the information from vibrational modes of a molecular bond. Infrared spectroscopy probes the vibrational states through absorption at the vibrational resonant frequency. Raman spectroscopy is based on the spontaneous Raman scattering from a molecule in which Stokes and anti-Stokes photons are spontaneously generated through the vibrational states excited by a pump beam (Figure 1E). Spontaneous Raman spectroscopy is often used to probe biological samples which contain numerous chemicals and macromolecules resulting in a complex vibrational spectrum. However, the scattering cross-section for spontaneous Raman is relatively small ($\sim 10^{-30}$ cm^2 per molecule) and thus requires a long exposure time to acquire an image. Techniques which take advantage of coherent interactions however may be applied to overcome this limitation.

Vibrational sum frequency generation (VSFG) is a generalized form of second harmonic generation, in which two photons of the frequency ω_1 and ω_2 are converted to a photon of the frequency $\omega_1 + \omega_2$ (Figure 1F). When ω_1 is tuned to match a vibrational transition, VSFG will be resonantly enhanced to probe the vibrational modes. Such a process involves both infrared absorption and the anti-Stokes Raman transition process, so the molecular vibrational mode must be both IR and Raman active to appear in a VSFG spectrum.[11]

Coherent anti-Stokes Raman scattering (CARS) is a four-wave mixing process that generates an anti-Stokes photon which is resonantly enhanced by vibrational transitions (Figure 1G). It was also discovered in the early days of nonlinear optics in 1965[12] but was not applied to spectroscopy until a decade later in 1974[13] due to the development of the high peak power tunable laser. Because CARS is a coherent process, the scattering cross-section is orders of magnitude higher than that of spontaneous Raman scattering and therefore is well-suited for high-speed imaging.[14,15]

Stimulated Raman scattering (SRS), reported in 1962,[16] was among the first nonlinear optical phenomena to be discovered. However, SRS was only recently appropriated to microscopy.[17−19] SRS is a two-photon process that leads to the excitation of a vibrational state. When both a pump and Stokes photon are used, the molecular vibration is coherently driven and the Raman process is greatly enhanced. During this process a pump photon is converted to a Stokes photon (Figure 1H). The loss of the pump photon is called simulated Raman loss (SRL), and the gain of the Stokes photon is called simulated Raman gain (SRG). Experimentally, both the effects of SRL and SRG can be detected.

The high intensity incident fields which these nonlinear optical processes require can be achieved by tightly focusing a high-power laser, typically an ultrafast pulsed laser, into the specimen. The nonlinear optical signal generated within the focal region can then be collected, appropriately filtered, and recorded. Microscopy is commonly performed by coupling the necessary excitation source or sources into a scanning microscope (Figure 2). The signal strength of these nonlinear processes is exponentially proportional to the incident field intensity which decays with the inverse square of the axial distance from the focal spot. This effect provides label-free nonlinear optical microscopy with intrinsic three-dimensional sectioning capabilities comparable to confocal microscopy or two-photon excitation fluorescence (TPEF) microscopy. The excitation beam is scanned in two or three dimensions through the sample and the signal is recorded for every point, after which an image is reconstructed with software (Figure 2 (inset)). Each technique requires a specific excitation and detection scheme which we will not discuss in detail here. Table 1 summarizes some important design parameters for each of these imaging modalities as well as the widely used epi-fluorescence and scanning-confocal microscopy for comparison (Table 1). The parameters listed in the table refer to typical configurations. The purpose of the following sections is to present the breadth of biological imaging applications made possible with these methods. In Table 1 and throughout this Feature we refer the reader to a vast literature for comprehensive descriptions and reviews of these applications, see for example ref 20.

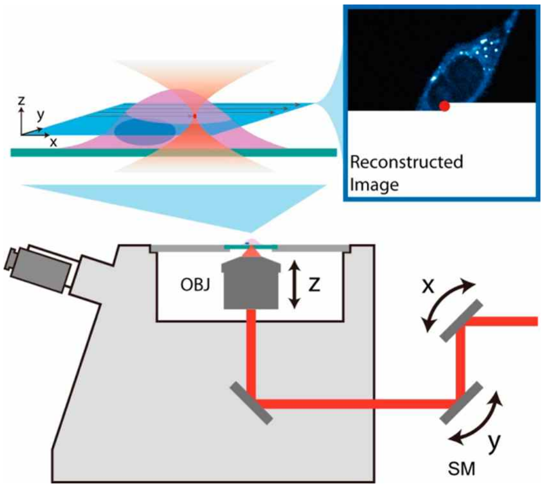

Figure 2. Schematic diagram of a typical nonlinear optical imaging configuration implemented in a scanning microscope. The excitation light is directed through two scanning mirrors (SM) which raster the focal spot across an $X-Y$ plane within the specimen. The height of the imaging plane is controlled by a vertical positioning stage on the objective (OBJ). At every point, the signal is recorded and used to reconstruct a three-dimensional image of the specimen.

NONLINEAR OPTICAL IMAGING AT THE SINGLE-CELL LEVEL

Over the past decade many advances have been made to the imaging modalities described above so that now there is a comprehensive toolbox of label-free nonlinear imaging techniques for a wide range of bioanalytical applications. Below we survey some contemporary applications of these imaging tools in order to highlight the factors one might consider when choosing the best technique or combination of techniques for their specific research endeavor.

Coherent Raman scattering (CRS) microscopy, which includes both CARS and SRS, has proven to be particularly powerful for studying lipid rich structures. The relatively isolated Raman peaks associated with vibrational states of the carbon−hydrogen bond, which are abundant in fatty acid molecules, provide a unique signature for lipids in the otherwise chemically diverse environment of a cell. Additionally the densely packed structure of a lipid body provides an especially strong signal for CRS microscopy. Such applications have been highlighted by many comprehensive reviews in the field; see for example refs 21−23.

When examining a dynamic process, like intercellular transport of lipid bodies, it is critical that the measurement system does not perturb the process under investigation. In the introduction we presented this as a primary benefit of label-free imaging methods; however, with the high-intensity, pulsed laser sources required for these techniques, it is fair to ask whether or not the excitation beam is harmful to the system that it is probing. Nan and colleagues showed that with careful consideration of excitation energy, CARS microscopy can be effectively used to monitor lipid droplet organelle transport in live cells while avoiding photo damage.[24] Without fluorescent labels they were able to track intercellular lipid droplet motion and quantify both diffusive and protein mediated transport in mouse adrenal cortical cells.

Nonperturbative long time scale live cell imaging is a powerful tool for studying dynamic biological processes, and with label-free techniques observation times are not limited by photo bleaching. Jüngst et al. used CARS microscopy to track lipid droplet formation and dynamics during adipogenesis, the process by which stem cells differentiate into adipocytes.[25] They monitored adipogenic lipid droplet formation and maturation over a 5 day period. Quantitative feature recognition and object tracking allowed them to observe lipid droplet fusion with enough accuracy to confirm previously proposed mechanisms of lipid transfer and propose a quantitative model.

Densely packed, large, lipid droplets are not the only lipid structure that can be observed by CRS however. In an early application of CARS microscopy, Potma and colleagues

Table 1. Comparison of Optical Imaging Techniques

	input	output	incident wavelength range (nm)	typical excitation source	detection scheme^b	label-free	3D	ref
epi-fluorescence	ω	$\omega' < \omega$	340−785	mercury lamp	CCD/EMCCD/CMOS cameras	no	no	
confocal				continuous wave laser	PMT, confocal pinhole	no	yes	
TPEF^a	ω	$\omega < \omega' < 2\omega$	550−1140	femtosecond laser	PMT	no	yes	69, 70
3PEF^a		$\omega < \omega' < 3\omega$	840−1140	femtosecond laser	PMT	no	yes	71
SHG		$\omega' = 2\omega$	550−1140	femtosecond laser	PMT	yes	yes	72−74
THG		$\omega' = 3\omega$	780−1500	femtosecond laser	PMT	yes	yes	75, 76
VSFG	ω_1, ω_2 ($\omega_1 = \Omega$)	$\omega' = \omega_1 + \omega_2$	400−600/2500−5000	femtosecond laser	PMT	yes	yes	11
CARS	ω_p, ω_s ($\omega_p - \omega_s = \Omega$)	$\omega' = \omega_{as}$	780−995/1064	picosecond/femtosecond laser	PMT	yes	yes	12, 15, 77
SRS		$\Delta I_p, \Delta I_s$			photodiode, demodulator	yes	yes	16, 17

^{a}TPEF, two photon excitation fluorescence; 3PEF, three photon excitation fluorescence. ^{b}CCD, charge-coupled device; EMCCD, electron multiplied charge-coupled device; CMOS, complementary metal-oxide-semiconductor; PMT, photomultiplier tube.

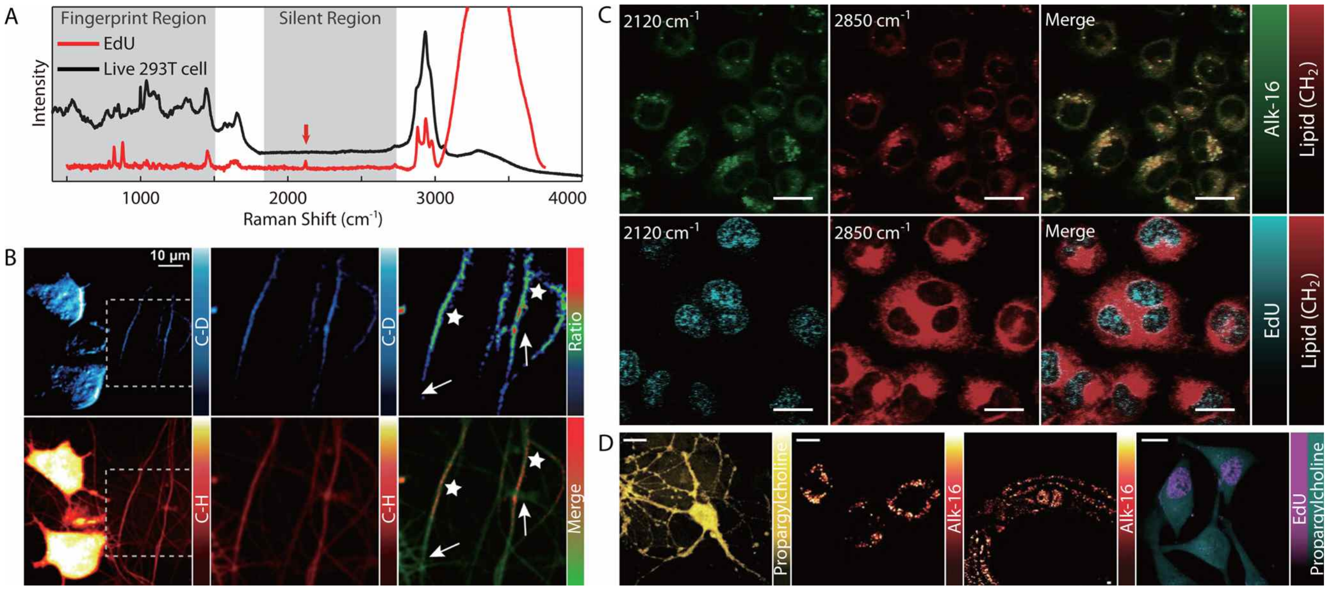

Figure 3. Chemical tagging for SRS imaging with high specificity: (A) representative Raman spectra of a single 293T cell (black) and an alkyne tagged 5-ethynyl-2′-deoxyuridine (EdU) solution (red). The red arrow indicates the peak associated with the alkyne group. The two gray patches indicate the fingerprint region and silent region. (B) Imaging newly synthesized protein in cultured neuronlike differentiable mouse neuroblastoma (N2A) cells. Deuterium labeled amino acid reveals new proteins in both cell bodies and neurites. The merged image (lower right) and ratio map (upper right) reveal the distribution of newly synthesized protein in neurites with regions of high and low contrast indicated with stars and arrows, respectively. Reprinted with permission from ref 41. Copyright 2013 National Academy of Sciences. (C) Probing alkyne labeled biomolecules in live Hela cells. Imaging at wave numbers 2120 cm^{-1} showed alkyne tagged lipid (Alk-16) or nucleic acid (EdU) signals, which are falsely colored green and blue, respectively, and imaging at 2850 cm^{-1} showed the intrinsic lipid signal (CH_2) represented in red. Scale bars are 20 μm. Reprinted with permission from ref 43. Copyright 2014 John Wiley & Sons, Inc. (D) Probing alkyne labeled propargylcholine (yellow and blue) and lipids (Alk-16) in cultured neurons, cells, and *C. elegans*. Scale bars are 10 μm. Reprinted with permission from ref 44. Copyright 2014 Macmillan Publishers Ltd.

demonstrated detection sensitivity high enough to image single lipid bilayers.[26]

It is often useful to simultaneously detect multiple chemical species within a cell. While this goal is commonly achieved with a variety of fluorescent labeling strategies, there is now a growing toolbox of methods aimed at achieving multicolor images without fluorescent labels. Perhaps the simplest approach to generating a multicolor image with CRS microscopy is to take sequential images while tuning the laser source to excite different Raman bands. Zhang et al., for example, acquired consecutive SRS images at multiple Raman bands in order to reveal both nucleic acids and lipids in live cells.[27] With this approach, the finite time associated with image acquisition as well as tuning of the excitation wavelength sets a limit on the imaging temporal resolution as anything that moves during the image acquisition will be blurry or misaligned between the channels.

Another strategy for achieving multichannel detection is to employ a multimodal configuration in which various imaging techniques are combined in a single microscope for simultaneous image acquisition. An early demonstration of nonlinear multimodal imaging of biological specimens was performed with second-harmonic generation and two photon excitation fluorescence.[28] This combination of techniques is popular because the same excitation source can be used for both imaging modalities and either the forward or backward scattered signal can be spectrally separated for simultaneous image collection. With similar advantages, second and third harmonic generation can be combined in a scanning microscope for noninvasive, label-free, multimodal imaging. Chu et al. used this combination to image cell proliferation in live zebra fish embryos.[29] THG was used to detect the inhomogeneities at the cell boundary and across the nuclear membrane and various internal organelles, while SHG resolved centrosomes and mitotic spindles during mitosis due to disruption of optical centro-symmetry in the otherwise ordered structures.

Mahou et al. also examined zebra fish embryos with a microscope that combined THG with four-wave mixing.[30] They then demonstrated an extension of the technique by adding SHG and TPEF. Soon thereafter Segawa et al. presented yet another demonstration of tetra-modal nonlinear microscopy by combining CARS, SHG, THG, and third-order SFG to image single cells with multiple channels.[31]

These examples illustrate the breadth of chemical and structural diversity that can be resolved with multimodal label-free microscopy. These technologies are thus most effectively used when the imaging apparatus is tailored to the biological system at hand. In many situations an investigation may indeed use a combination of fluorescence microscopy and label-free microscopy. In order to study enzyme digestion of biomass, Ding and colleagues used scanning confocal microscopy and two-color SRS as well as bright field microscopy and atomic force microscopy.[32] Fluorescent labeling was used to identify the plant cell walls and exposed cellulose surfaces while SRS resolved lignins and polysaccharides. While these two imaging modalities were not used simultaneously, the authors were nonetheless able to quantify the role of lignins and polysaccharides during the enzyme assisted degradation of plant matter.

The distinctive Raman spectrum allows lipid rich structures to be uniquely resolved with a single CRS imaging channel. In order to resolve chemicals with overlapping vibrational spectra including proteins and nucleic acids whose spectral signature lie largely in the "fingerprint region" (Figure 3), it is necessary to image with multiple Raman bands. Chemical signals can then be separated by decomposition of the multiplexed image with a linear combination of spectral intensities.[33]

Multiplexed CRS microscopy is another quickly maturing technique for multichannel and hyperspectral imaging. Fu et al. demonstrated multiplex SRS using a broadband femtosecond laser as the pump source.[34] They modulated three wavelength regions with different frequencies and separated the three detection channels in the frequency domain for simultaneous multicolor imaging. Recently, Fu et al. used another hyperspectral approach[35] to map the composition of neutral lipid droplets in live cells.[36] There are a number of approaches to hyperspectral coherent Raman imaging, and a more comprehensive review of these techniques can be found in refs 23 and 37.

Multicolor CRS microscopy allows for the decomposition of signal from chemicals with overlapping spectra, including those whose dominant peaks lie predominantly in the fingerprint region. There is a limit, however, to the specificity that coherent Raman techniques can provide. Different proteins, for example, exhibit very subtle if not completely immeasurable differences in their Raman spectrum. One strategy to achieve high specificity while avoiding large fluorescent molecule labels is to label proteins or cellular components of interest with small tags which have distinct vibrational signatures. Such chemical tags are often defined by specific chemical bonds or isotopes[36,38] which have unique Raman peaks. Deuterium, alkyne, and azide, for example, all display a Raman peak in the "silent region" of the spectrum, a spectral region in which cells typically do not have any significant Raman peaks (Figure 3A).

Yasui and colleagues used the Raman shift associated with deuterated water to differentiate the water inside and outside single cells or embryos to study the diffusion dynamics of free water.[39,40] Similarly, by culturing cells with deuterium labeled amino acid, Wei et al. imaged newly synthesized protein in cultured neurons[41] (Figure 3B). These demonstrations take advantage of the Raman peak shifts associated with isotopes to differentiate the chemical analogues. Furthermore, Min and his colleagues showed deuterium labeled choline can reveal itself and its metabolites in neurons with SRS.[42] Min's group and our group have shown that alkyne can be used as a bio-orthogonal label to offer specificity to various biomolecules, like nucleic acid, lipid, amino acid, and glycans[43,44] (Figure 3C,D). We were able to probe palmitic acid in live cells, without the spectral crosstalk that would otherwise occur between molecules with overlapping Raman spectra. Molecules like nucleic acids whose Raman signature is buried in fingerprint region could also be revealed with the increased signal provided by alkyne groups. With the use of small chemical tags, CRS offers enhanced chemical specificity with minimal perturbation of the system, which is important in many current biological research endeavors.

QUANTITATIVE BIOLOGICAL IMAGING AT THE SINGLE-CELL LEVEL

The high contrast and chemical specificity of fluorescent imaging combined with the development of high-throughput, multiparameter image acquisition technology has enabled researchers to pursue more quantitative approaches to image analysis. In the same way that the revolution in genetic sequencing technology has recruited computer scientists to devise methods to analyze large amounts of genetic information, the evolution of biological imaging technology requires advanced algorithms for processing large volumes of information rich biological images. There are two major goals of biological image processing, data extraction and data management. While images of cells tend to give scientists an intuitive understanding of the structure and the spatial distributions of chemicals and organelles, identification and quantification of such parameters are necessary in order to accurately compare images and make objective conclusions about an experiment. Moreover these extracted data can provide a quantitative understanding of the diversity of cellular characteristics and allow researchers to analyze the statistical distribution of parameters in a population of cells at the single-cell level.

Data management becomes an important consideration because contemporary automated imaging platforms are now capable of performing time-lapse imaging on multiple samples in which each data point can consist of a three-dimensional stack of high-resolution images with multiple detection channels.[3] It is impractical and in many cases impossible for a human to manually process such large amounts of data so we typically rely on automated image processing pipelines to manage these sets of images and reduce them to annotated data sets that can be more readily mined for information.

With these goals in mind, there have been great efforts to produce capable and user-friendly software, ranging from open source platforms like ImageJ[45] or CellProfiler,[46] to commercial image processing libraries like the Image Processing Toolbox in Matlab. In a recent focus on "Bioimage Informatics", Eliceiri et al. reviewed the landscape of current available biological image processing software tools.[47]

The multiplexed and multimodal nonlinear imaging techniques described here enable three-dimensional cellular imaging with unprecedented speed and chemical specificity, and in many aspects these techniques are approaching the versatility of fluorescence microscopy. In fact, in the larger context of biomedical imaging, it is more instructive to categorize nonlinear imaging techniques as complementary to fluorescence microscopy. Applying advanced image processing and analysis to extract quantitative information from label-free images is thus a natural extension of the technology. There is now a growing literature in which established image processing algorithms have been adapted to the contrast mechanisms yielded by nonlinear microscopy.

One of the primary tasks in quantitative image analysis of single cells, which is often necessary before other procedures can be executed, is image segmentation. The goal in image segmentation is to divide an entire field of view into discrete areas that represent meaningful objects, for example, distinguishing individual cells in a tissue or colony. Additionally segmentation is used to partition organelles and structures *within* a cell as well. With fluorescence microscopy it is common to label biological molecules associated with specific regions of the cell like the cell membrane, cytoplasm, or nucleus, in order to facilitate segmentation. In such cases certain fluorescence channels can be used with minimal processing as a mask for inter- and intra-cell segmentation.[3]

With label-free nonlinear optical imaging segmentation must be tailored to the intrinsic contrast modality. For example, because of the low levels of lipid molecules in the cell nucleus, CARS microscopy tuned to excite the CH_2 vibrational band can be used to perform automated nuclear segmentation in tissue samples.[48] This approach has been extended to quantitatively classify tissue samples for differential diagnosis of lung cancer.[49,50] Multichannel imaging can also be used with label-free techniques to simplify segmentation. For example, combining CARS and autofluorescence excited by TPEF enabled identification of nuclei locations and cell boundaries using the pixel intensities to locate nuclei and pixel gradients to detect cell boundaries.[51]

As we have discussed above, many applications of label-free nonlinear optical microscopy involve imaging lipid rich structures within cells. Naturally, such structures can thus be automatically identified and parametrized with the appropriate implementation of quantitative image processing. With CARS microscopy, for example, careful evaluation and selection of processing algorithms can lead to accurate segmentation of lipid droplets.[52] Combining lipid identification with nuclei or cell boundary segmentation is a powerful way to measure lipid accumulation at the single-cell level.[52] Lipid analysis at the single-cell level allows for quantification of heterogeneity in cellular populations. Le and Cheng combined single-cell CARS microscopy with flow cytometry, TPEF, and quantitative real-time PCR to assess phenotypic heterogeneity in differentiating adipocytes.[53] With this approach they measured correlations in gene expression and adipogenic progression with single cell resolution.

THG also provides significant contrast for detecting the surface of lipid droplets because of the difference in nonlinear optical properties across the interface of dense lipid bodies and the surrounding cell cytoplasm. In this way THG was used to segment intercellular lipid droplets and reconstruct the three-dimensional spatial distribution of these lipid bodies in rat liver cells.[54] With this data, the size distribution of lipid droplets in normal and regenerating hepatocytes were quantitatively compared. Lipid-rich neuronal structures like axons, dendrites, and myelin sheaths offer another potential source of contrast for imaging intact brain tissue with THG. The mismatched length scale of lipid structures inside and outside the neuron bodies can be exploited through tuning of the scanning focal spot size in order to create a "shadow contrast" image in which single neurons can be clearly identified and counted with automated image analysis routines.[55]

Applying quantitative image processing and label-free imaging to the study of embryogenesis, Oliver et al. used SHG and THG to monitor unstained whole developing zebrafish embryos.[56] SHG was used to detect mitosis events by identifying the mitotic spindle during metaphase and THG was used to image the cell boundaries and quantify cell shape (Figure 4A–J). The 400 μm penetration depth, micrometer spatial resolution, and minute-temporal resolution provided by

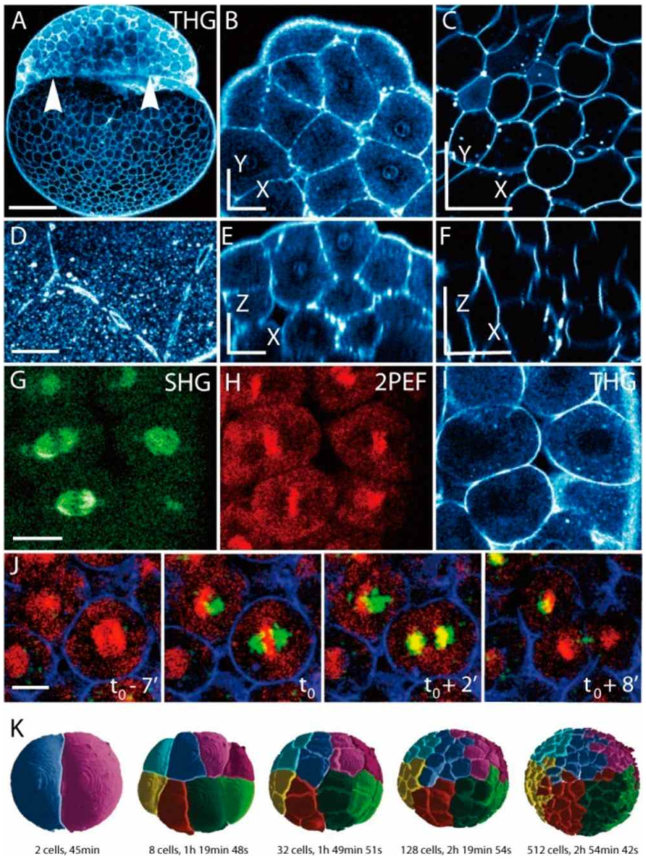

Figure 4. Multimodal nonlinear optical imaging of a developing zebra fish embryo. (A) Cross-sectional THG image at the 512-cell stage. White arrows indicate the yolk-blastoderm interface. Scale bar 200 μm. (B–F) $X-Y$ and $Z-X$ projections of Blastoderm cells (B, D and E) and yolk platelets (C and F). Mitosis events imaged with SHG (G) TFEP (H) and THG (I). The scale bar is 20 μm. (J) A temporal sequence capturing mitosis with merged SHG, TPEF, and THG images. (K) A digital reconstruction of the embryo with single-cell segmentation from the 1-cell stage to the 512-cell stage. Reprinted with permission from ref 56. Copyright 2010 AAAS.

these imaging modalities enabled the authors to track cell division and the single-cell level and reconstruct a precise lineage tree along with a three-dimensional dynamic atlas of the developing embryo through the first 10 cycles of cell division (Figure 4L). Together these studies demonstrate a powerful and emerging approach to quantitative bioimaging at the single-cell level.

OUTLOOK

The increase in information content enabled by multiparameter imaging and automated analysis of single cells is accompanied by a significant increase in data volume. When exploring biology at the single-cell level, significantly more data points are required to assess a given system like a tissue sample or cellular network. It makes sense to readdress experimental design as well as the image collection and analysis techniques to ensure that the experimental throughput matches that of the imaging system. Microfluidic technology provides an effective platform for systematic single cell manipulation and analysis.[57,58] With multilayer soft lithography,[59] it is possible to construct integrated devices containing arrays of cell chambers for live-cell time lapse imaging.[60−66] This technology has proven to be a useful platform for high-throughput quantitative single cell fluorescent imaging,[67] and we suggest that nonlinear imaging will similarly benefit from microfluidic integration. CARS has already been combined with microfluidic flow channels to perform label-free flow cytometry.[68] Microfluidic cell culture arrays and devices for single-cell manipulation provide microscopists with an efficient way to perform multiplexed high-throughput cellular imaging experiments. As these complementary approaches continue to evolve, life science researchers will be able to form a clearer picture of the complexity of life at the single cell level.

AUTHOR INFORMATION

Corresponding Author

*E-mail: yanyi@pku.edu.cn.

Notes

The authors declare no competing financial interest.

Biographies

Dr. Aaron Streets received his Ph.D. in applied physics from Stanford University. He currently holds a postdoctoral research position in the Biodynamic Optical Imaging Center at Peking University. His research involves the integration of optical analysis and imaging with microfluidic technology to study biological and biophysical systems.

Ang Li is currently a research assistant at Peking University. He graduated from Peking University with a B.S. in Physics in 2013. His research focuses on optimizing the detection system of stimulated Raman scattering microscopy.

Tao Chen is a Ph.D. candidate in the College of Engineering at Peking University. He received his Bachelor's degree in Physics from Peking University. He currently is working on nonlinear optical microscopy, with a focus on transient absorption microscopy and stimulated Raman scattering microscopy. With these techniques, he studies the interaction between nanoparticles and cells and the use of chemical tags for coherent Raman imaging in biological environments.

Prof. Yanyi Huang received his B.S. (Chemistry) and Sc.D. (Inorganic Chemistry) from Peking University in 1997 and 2002, respectively. He worked at Caltech with Amnon Yariv (Postdoc in Applied Physics) and then moved to Stanford with Stephen Quake (Postdoc in Bioengineering). He joined the Peking University faculty in 2006. He is Professor in the College of Engineering and Principal Investigator and Associate Director of Biodynamic Optical Imaging Center (BIOPIC). His current research interests are microfluidics, microscopy, and high-throughput sequencing.

ACKNOWLEDGMENTS

This work was supported by the Ministry of Science and Technology of China (Grant 2011CB809106) and the National Natural Science Foundation of China (Grants 21222501 and 91313302). A.M.S. was supported by the Whitaker International Biomedical Engineering Fellowship.

REFERENCES

(1) Zhu, J.; Paul, W. E. *Cell Res.* **2010**, *20*, 4−12.
(2) Losick, R.; Desplan, C. *Science* **2008**, *320*, 65−68.
(3) Muzzey, D.; van Oudenaarden, A. *Annu. Rev. Cell Dev. Biol.* **2009**, *25*, 301−327.
(4) Ji, M.; Orringer, D. A.; Freudiger, C. W.; Ramkissoon, S.; Liu, X.; Lau, D.; Golby, A. J.; Norton, I.; Hayashi, M.; Agar, N. Y. R.; Young, G. S.; Spino, C.; Santagata, S.; Camelo-Piragua, S.; Ligon, K. L.; Sagher, O.; Xie, X. S. *Sci. Transl. Med.* **2013**, *5*, 201ra119.
(5) Bloembergen, N. *Nonlinear Optics*, 4th ed.; World Scientific Publishing Co. Pte. Ltd.: River Edge, NJ, 1996.
(6) Shen, Y. R. *The Principles of Nonlinear Optics*; John Wiley & Sons: Hoboken, NJ, 2003.
(7) Campagnola, P. J.; Loew, L. M. *Nat. Biotechnol.* **2003**, *21*, 1356−1360.
(8) Campagnola, P. J.; Millard, A. C.; Terasaki, M.; Hoppe, P. E.; Malone, C. J.; Mohler, W. A. *Biophys. J.* **2002**, *82*, 493−508.
(9) Zipfel, W. R.; Williams, R. M.; Christie, R.; Nikitin, A. Y.; Hyman, B. T.; Webb, W. W. *Proc. Natl. Acad. Sci. U.S.A.* **2003**, *100*, 7075−7080.
(10) Yelin, D.; Silberberg, Y. *Opt. Express* **1999**, *5*, 169−175.
(11) Wang, H.-F.; Gan, W.; Lu, R.; Rao, Y.; Wu, B.-H. *Int. Rev. Phys. Chem.* **2005**, *24*, 191−256.
(12) Maker, P. D.; Terhune, R. W. *Phys. Rev.* **1965**, *137*, A801−A818.
(13) Begley, R. F.; Harvey, A. B.; Byer, R. L. *Appl. Phys. Lett.* **1974**, *25*, 387−390.
(14) Evans, C. L.; Potma, E. O.; Puoris'haag, M.; Cote, D.; Lin, C. P.; Xie, X. S. *Proc. Natl. Acad. Sci. U.S.A.* **2005**, *102*, 16807−16812.
(15) Zumbusch, A.; Holtom, G. R.; Xie, X. *Phys. Rev. Lett.* **1999**, *82*, 4142−4145.
(16) Woodbury, E. J.; N, W. *Proc. Inst. Radio Eng.* **1962**, *50*, 2367.
(17) Freudiger, C. W.; Min, W.; Saar, B. G.; Lu, S.; Holtom, G. R.; He, C.; Tsai, J. C.; Kang, J. X.; Xie, X. S. *Science* **2008**, *322*, 1857−1861.
(18) Nandakumar, P.; Kovalev, A.; Volkmer, A. *New J. Phys.* **2009**, *11*, 033026.
(19) Ozeki, Y.; Dake, F.; Kajiyama, S. a. i.; Fukui, K.; Itoh, K. *Opt. Express* **2009**, *17*, 3651−3658.
(20) Meyer, T.; Schmitt, M.; Dietzek, B.; Popp, J. R. *J. Biophoton.* **2013**, *6*, 887−904.
(21) Folick, A.; Min, W.; Wang, M. C. *Current Opin. Genetics Dev.* **2011**, *21*, 585−590.
(22) Le, T. T.; Yue, S.; Cheng, J.-X. *J. Lipid Res.* **2010**, *51*, 3091−3102.
(23) Zumbusch, A.; Langbein, W.; Borri, P. *Prog. Lipid Res.* **2013**, *52*, 615−632.
(24) Nan, X.; Potma, E. O.; Xie, X. S. *Biophys. J.* **2006**, *91*, 728−735.
(25) Jüngst, C.; Klein, M.; Zumbusch, A. *J. Lipid Res.* **2013**, *54*, 3419−3429.
(26) Potma, E. O.; Xie, X. S. *J. Raman Spectrosc.* **2003**, *34*, 642−650.
(27) Zhang, X.; Roeffaers, M. B. J.; Basu, S.; Daniele, J. R.; Fu, D.; Freudiger, C. W.; Holtom, G. R.; Xie, X. S. *ChemPhysChem* **2012**, *13*, 1054−1059.
(28) Gauderon, R.; Lukins, P. B.; Sheppard, C. J. R. *Micron* **2001**, *32*, 685−689.

(29) Chu, S.-W.; Chen, S.-Y.; Tsai, T.-H.; Liu, T.-M.; Lin, C.-Y.; Tsai, H.-J.; Sun, C.-K. *Opt. Express* **2003**, *11*, 3093−3099.

(30) Mahou, P.; Olivier, N.; Labroille, G.; Duloquin, L.; Sintes, J.-M.; Peyriéras, N.; Legouis, R.; Débarre, D.; Beaurepaire, E. *Biomed. Opt. Express* **2011**, *2*, 2837.

(31) Segawa, H.; Okuno, M.; Kano, H.; Leproux, P.; Couderc, V.; Hamaguchi, H.-o. *Opt. Express* **2012**, *20*, 9551−9557.

(32) Ding, S.-Y. Y.; Liu, Y. S.; Zeng, Y.; Himmel, M. E.; Baker, J. O.; Bayer, E. A. *Science* **2012**, *338*, 1055−1060.

(33) Yu, Z.; Chen, T.; Zhang, X.; Fu, D.; Liao, X.; Shen, J.; Liu, X.; Zhang, B.; Xie, X. S.; Su, X.-D.; Chen, J.; Huang, Y. *Chem. Sci.* **2012**, *3*, 2646.

(34) Fu, D.; Lu, F. K.; Zhang, X.; Freudiger, C.; Pernik, D. R.; Holtom, G.; Xie, X. S. *J. Am. Chem. Soc.* **2012**, *134*, 3623−3626.

(35) Fu, D.; Holtom, G. R.; Freudiger, C.; Zhang, X.; Xie, X. S. *J. Phys. Chem. B* **2013**, *117*, 4634−4640.

(36) Fu, D.; Yu, Y.; Folick, A.; Currie, E.; Farese, R. V.; Tsai, T.-H.; Xie, X. S.; Wang, M. C. *J. Am. Chem. Soc.* **2014**, *136*, 8820−8828.

(37) Chung, C.-Y.; Potma, E. O. *Annu. Rev. Phys. Chem.* **2013**, *64*, 77−99.

(38) Shen, Y.; Xu, F.; Wei, L.; Hu, F.; Min, W. *Angew. Chem., Int. Ed.* **2014**, *53*, 5596−5599.

(39) Ibata, K.; Takimoto, S.; Morisaku, T.; Miyawaki, A.; Yasui, M. *Biophys. J.* **2011**, *101*, 2277−2283.

(40) Yu, Y. C.; Sohma, Y.; Takimoto, S.; Miyauchi, T.; Yasui, M. *Sci. Rep.* **2013**, *3*, 2745.

(41) Wei, L.; Yu, Y.; Shen, Y.; Wang, M. C.; Min, W. *Proc. Natl. Acad. Sci. U.S.A.* **2013**, *110*, 11226−11231.

(42) Hu, F.; Wei, L.; Zheng, C.; Shen, Y.; Min, W. *Analyst* **2014**, *139*, 2312−2317.

(43) Hong, S.; Chen, T.; Zhu, Y.; Li, A.; Huang, Y.; Chen, X. *Angew. Chem., Int. Ed.* **2014**, *53*, 5827−5831.

(44) Wei, L.; Hu, F.; Shen, Y.; Chen, Z.; Yu, Y.; Lin, C.-C.; Wang, M. C.; Min, W. *Nat. Methods* **2014**, *11*, 410−412.

(45) Schneider, C. A.; Rasband, W. S.; Eliceiri, K. W. *Nat. Methods* **2012**, *9*, 671−675.

(46) Carpenter, A.; Jones, T.; Lamprecht, M.; Clarke, C.; Kang, I.; Friman, O.; Guertin, D.; Chang, J.; Lindquist, R.; Moffat, J.; Golland, P.; Sabatini, D. *Genome Biol.* **2006**, *7*, R100.

(47) Eliceiri, K. W.; Berthold, M. R.; Goldberg, I. G.; Ibáñez, L.; Manjunath, B. S.; Martone, M. E.; Murphy, R. F.; Peng, H.; Plant, A. L.; Roysam, B.; Stuurmann, N.; Swedlow, J. R.; Tomancak, P.; Carpenter, A. E. *Nat. Methods* **2012**, *9*, 697−710.

(48) Hammoudi, A.; Li, F.; Gao, L.; Wang, Z.; Thrall, M.; Massoud, Y.; Wong, S. C. In *Machine Learning in Medical Imaging*; Suzuki, K., Wang, F., Shen, D., Yan, P., Eds.; Springer: Berlin Heidelberg, Germany, 2011; Vol. *7009*, pp 317−325.

(49) Gao, L.; Hammoudi, A. A.; Li, F.; Thrall, M. J.; Cagle, P. T.; Chen, Y.; Yang, J.; Xia, X.; Fan, Y.; Massoud, Y.; Wang, Z.; Wong, S. T. C. *J. Biomed. Opt.* **2012**, *17*, 0660171−06601711.

(50) Gao, L.; Li, F.; Thrall, M. J.; Yang, Y.; Xing, J.; Hammoudi, A. A.; Zhao, H.; Massoud, Y.; Cagle, P. T.; Fan, Y.; Wong, K. K.; Wang, Z.; Wong, S. T. C. *J. Biomed. Opt.* **2011**, *16*, 096004−096010.

(51) Medyukhina, A.; Meyer, T.; Schmitt, M.; Romeike, B. F. M.; Dietzek, B.; Popp, J. *J. Biophoton.* **2012**, *5*, 878−888.

(52) Chen, W. W.; Chien, C. H.; Wang, C. L.; Wang, H. H.; Wang, Y. L.; Ding, S. T.; Lee, T. S.; Chang, T. C. *Anal. Bioanal. Chem.* **2013**, *405*, 8549−8559.

(53) Le, T. T.; Cheng, J.-X. *PLoS One* **2009**, *4*, e5189.

(54) Débarre, D.; Supatto, W.; Pena, A.-M.; Fabre, A.; Tordjmann, T.; Combettes, L.; Schanne-Klein, M.-C.; Beaurepaire, E. *Nat. Methods* **2006**, *3*, 47−53.

(55) Witte, S.; Negrean, A.; Lodder, J. C.; de Kock, C. P.; Testa Silva, G.; Mansvelder, H. D.; Louise Groot, M. *Proc. Natl. Acad. Sci. U.S.A.* **2011**, *108*, 5970−5975.

(56) Olivier, N.; Luengo-Oroz, M. A.; Duloquin, L.; Faure, E.; Savy, T.; Veilleux, I.; Solinas, X.; Debarre, D.; Bourgine, P.; Santos, A.; Peyrieras, N.; Beaurepaire, E. *Science* **2010**, *329*, 967−971.

(57) Lecault, V.; White, A. K.; Singhal, A.; Hansen, C. L. *Curr. Opin. Chem. Biol.* **2012**, *16*, 381−390.

(58) Streets, A. M.; Huang, Y. *Biomicrofluidics* **2013**, *7*, 011302.

(59) Unger, M. A.; Chou, H. P.; Thorsen, T.; Scherer, A.; Quake, S. R. *Science* **2000**, *288*, 113−116.

(60) Balagadde, F. K.; You, L.; Hansen, C. L.; Arnold, F. H.; Quake, S. R. *Science* **2005**, *309*, 137−140.

(61) Gomez-Sjoberg, R.; Leyrat, A. A.; Pirone, D. M.; Chen, C. S.; Quake, S. R. *Anal. Chem.* **2007**, *79*, 8557−8563.

(62) Lecault, V.; Vaninsberghe, M.; Sekulovic, S.; Knapp, D. J.; Wohrer, S.; Bowden, W.; Viel, F.; McLaughlin, T.; Jarandehei, A.; Miller, M.; Falconnet, D.; White, A. K.; Kent, D. G.; Copley, M. R.; Taghipour, F.; Eaves, C. J.; Humphries, R. K.; Piret, J. M.; Hansen, C. L. *Nat. Methods* **2011**, *8*, 581−586.

(63) Hung, P. J.; Lee, P. J.; Sabounchi, P.; Aghdam, N.; Lin, R.; Lee, L. P. *Lab Chip* **2005**, *5*, 44−48.

(64) Hung, P. J.; Lee, P. J.; Sabounchi, P.; Lin, R.; Lee, L. P. *Biotechnol. Bioeng.* **2005**, *89*, 1−8.

(65) Mehling, M.; Tay, S. *Curr. Opin. Biotechnol.* **2014**, *25*, 95−102.

(66) Zheng, C.; Chen, G. E.; Pang, Y.; Huang, Y. *Sci. China Chem.* **2012**, *55*, 502−507.

(67) Tay, S.; Hughey, J. J.; Lee, T. K.; Lipniacki, T.; Quake, S. R.; Covert, M. W. *Nature* **2010**, *466*, 267−271.

(68) Wang, H.-W.; Bao, N.; Le, T. L.; Lu, C.; Cheng, J.-X. *Opt. Express* **2008**, *16*, 5782.

(69) Denk, W.; Strickler, J.; Webb, W. *Science* **1990**, *248*, 73−76.

(70) Drobizhev, M.; Makarov, N. S.; Tillo, S. E.; Hughes, T. E.; Rebane, A. *Nat. Methods* **2011**, *8*, 393−399.

(71) Hell, S. W.; Malak, H. M.; Gryczynski, I.; Lakowicz, J. R.; Bahlmann, K.; Schrader, M.; Soini, A. *J. Biomed. Opt.* **1996**, *1*, 71−74.

(72) Franken, P.; Hill, A.; Peters, C.; Weinreich, G. *Phys. Rev. Lett.* **1961**, *7*, 118−119.

(73) Gannaway, J. N.; Sheppard, C. J. R. *Opt. Quantum Electron.* **1978**, *10*, 435−439.

(74) Hellwarth, R.; Christensen, P. *Opt. Commun.* **1974**, *12*, 318−322.

(75) Barad, Y.; Eisenberg, H.; Horowitz, M.; Silberberg, Y. *Appl. Phys. Lett.* **1997**, *70*, 922−924.

(76) Muller; Squier; Wilson; Brakenhoff. *J. Microsc.* **1998**, *191*, 266−274.

(77) Duncan, M. D.; Reintjes, J.; Manuccia, T. J. *Opt. Lett.* **1982**, *7*, 350−352.